Energy Reports xxx (xxxx) xxx

Contents lists available at ScienceDirect

Energy Reports

journal homepage: www.elsevier.com/locate/egyr

Cylinder pressure based calibration model for engines using ethanol, hydrogen and natural gas as alternative fuels

Sami Massalami Mohammed Elmassalami Ayad [a,*], Carolina Locatelli Vago [a], Carlos Rodrigues Pereira Belchior [a], José Ricardo Sodré [b]

[a] Federal University of Rio de Janeiro, Department of Mechanical Engineering, Cidade Universitária, Ilha do Fundão, 21945-970, Rio de Janeiro, RJ, Brazil

[b] Department of Mechanical Engineering, Biomedical Engineering and Design, College of Engineering and Physical Sciences, Aston University, Birmingham, B4 7ET, UK

ARTICLE INFO

Article history:
Received 31 December 2020
Received in revised form 11 May 2021
Accepted 1 June 2021
Available online xxxx

Keywords:
Engine simulation
Calibration model
Cylinder pressure
Alternative fuels
Ethanol conversion
Hydrogen energy

ABSTRACT

This paper proposes a novel virtual engine calibration method for alternative fuels using thermodynamic simulation for in-cylinder pressure prediction. Based on known engine data, including the crank angle of the peak cylinder pressure, the optimization problem is defined for a desired indicated mean effective pressure. The decision variables are the combustion and heat transfer model parameters The method was tested for three different engines of different sizes, operating with ethanol, hydrogen and natural gas, and different equivalence ratios. The Wiebe model and a quasi-dimensional fractal combustion model were compared. The results showed that the method was able to successfully predict the in-cylinder pressure curve, with a coefficient of determination higher than 0.99. Furthermore, the method predicted the peak pressure and the crank angle corresponding to 50% of mass fraction burned with a maximum deviation of 2.5% and 1.5 °CA, respectively.

1. Introduction

It is common knowledge that national economic growth directly relates to its energy consumption, which strongly correlates with its pollutant emissions. These emissions, in turn, are related to issues like global warming and other environmental problems. Fossil fuels, the primary energy source used today, are responsible for the majority of greenhouse gas (GHG) and carbon dioxide (CO_2) emissions (IEA, 2016a,b). Thus, there is interest in replacing fossil fuels and finding alternative ways to achieve sustainable economic growth while also meeting stringent pollutant emission requirements. Therefore, the use of alternative fuels addresses not only concerns about energy security but also the environment. Among the alternatives, biofuels are strong candidates whose adoption foments growth in the rural sector and foreign exchange savings (Demirbas, 2007).

Biofuel refers to a liquid or gaseous fuel predominantly produced from biomass, such as ethanol, methanol, biodiesel, and gaseous fuels, such as hydrogen and methane (Demirbas, 2008). These fuels are readily available, represent a CO_2 cycle in combustion, are biodegradable, contribute to sustainability, and have a more environmentally friendly potential (Puppán, 2002). However, when compared to fossil fuels, the main disadvantage of biofuels is their performance, as they generally produce fewer emissions (de Faria et al., 2017). However, depending on the source and its composition, engine operation with these fuels requires extensive investigations to optimize it (Shivapuji and Dasappa, 2017; Matuszewska et al., 2016). This optimization consists of calibrating the engine electronic control unit (ECU), which usually uses lookup tables to control the engine operation (Isermann, 2014; Xin, 2011). However, experimental calibration usually involves many resources, people, facilities and funds (de Faria et al., 2017).

To this end, virtual engine calibration presents a cost-effective solution to these problems by permitting extensive parametric engine studies without the physical infrastructure requirements and can be a potent tool in engine development (Shivapuji and Dasappa, 2017). According to Grasreiner (2012), the term "virtual calibration" refers to the use of simulation methods instead of experimental measurements to develop the engine's ideal operation map (Jacob and Ashok, 2020). Of particular interest to this research is model-based calibration, in which virtual predictive modeling approaches are crucial (Jacob and Ashok, 2020).

* Corresponding author.
E-mail addresses: sami.ayad@mecanica.coppe.ufrj.br (S.M.M.E. Ayad), carolina.vago@ufrj.br (C.L. Vago), belchior@oceanica.ufrj.br (C.R.P. Belchior), j.sodre@aston.ac.uk (J.R. Sodré).

https://doi.org/10.1016/j.egyr.2021.06.015

For over half a century (Caton, 2018), internal combustion engines have been numerically modeled regarding their thermodynamic nature or with a complete fluid movement analysis (Heywood, 1988). Thus, it is possible to separate internal combustion simulations into three main categories (Caton, 2018):

- Zero-dimensional thermodynamic simulation of the engine operation cycle
- Quasi-dimensional thermodynamic simulation of the engine operation cycle
- Multi-dimensional or computational fluid dynamics (CFD) simulation

Each of these categories has its advantages and disadvantages as tools to understand engine operation. Multidimensional simulation describes physical events throughout time and space. CFD simulation provides more detailed information about the combustion process at the expense of high computational cost and is not in this work's scope.

Zero-dimensional simulation is simpler, faster and well suited for intensive parametric studies, in which a vast range of parameter values are investigated (Caton, 2018). A limitation of zero-dimensional models is that they depend on heat release profiles, which means that although they can accurately represent a particular fuel under specific operating conditions, they are not accurate when these conditions change (Shivapuji and Dasappa, 2017). Therefore, these models require more experimental tests to recalibrate the model for changes in the operating condition. Several authors have simulated engines operating with biofuels such as natural gas, biogas, ethanol, biodiesel, hydrogen and their blends using these models (Shivapuji and Dasappa, 2017; de Faria et al., 2017; Melo, 2007, 2012; Yeliana et al., 2011; Rocha, 2016; Reyes et al., 2013, 2016). Yeliana et al. (2011) used five different methods to adjust Wiebe equation parameters based on experimental mass fraction burned and heat release rate (HRR). They have found that the best strategy to calibrate these parameters was to adjust the shape parameter m, the crank angle corresponding to 90% of mass fraction burned (MFB), CA_{90}, and adding a correction parameter b. Reyes et al. (2013, 2016) used a genetic algorithm to both study cycle-by-cycle variation and characterize the combustion process of a spark ignition engine operating with methane–hydrogen mixtures. For this purpose, they have used both one and two zone combustion models and experimental pressure traces to obtain MFB curves.

Rocha (2016) proposed the use of an optimization method to estimate the Wiebe equation parameters in the simulation of hydrogen addition to biodiesel mixtures in a single-cylinder compression ignition (CI) engine. The objective functions were specific fuel consumption (SFC) and effective power and results showed reasonable deviations from experimental results, with maximum difference between simulated and experimental results for SFC, power, and in-cylinder peak pressure of 7.4%, 8.5%, and 6.5%, respectively. A zero-dimensional simulation was used to simulate methane and hydrogen methane mixtures using traditional Wiebe equation and a Double Wiebe equation (Yıldız and Çeper, 2017). The results showed that double Wiebe function was better in predicting the pressure curve after fitting the function coefficients to the MFB curve.

On the other hand, quasi-dimensional engine modeling is a compromise between accuracy and computational cost, and can provide deeper insights into the combustion process than zero-dimensional models. These improve zero-dimensional models and model the in-cylinder heat release as a turbulent combustion process, making it flexible with regards to changes in engine conditions (Shivapuji and Dasappa, 2017; De Bellis et al., 2017). They are used to predict the turbulent combustion (Reyes et al., 2015), the evolution of thermal parameters and the optimal ignition timing, flame behavior near the walls (Pashaei and Khoshbakhti Saray, 2019), and the combustion process in general (Mehra et al., 2018; Ma et al., 2008). Tinaut et al. (2011) used a quasi dimensional model to predict NOx formation through the combustion chamber geometry, flame speed correlations, optimal ignition timing, and ratio between laminar and turbulent velocities. The authors concluded that this approach was adequate in predicting the behavior of an engine running under similar conditions.

The use of quasi-dimensional models with biofuels require further model calibration or extrapolating correlations for the biofuels (Shivapuji and Dasappa, 2017; Mehra et al., 2018; Ma et al., 2008; Scala et al., 2016; Vancoillie et al., 2014; Verhelst et al., 2011; Ji et al., 2016). Using a quasi-dimensional approach with the eddy entrainment laminar burn-up concept to numerically investigate a syngas fueled engine, the simulation results agreed within 5% of the experimental data as long as the parametric variations were within the calibration regimes (Shivapuji and Dasappa, 2017). The application of a quasi-dimensional model to simulate butanol–gasoline blends on a spark ignition engine operating on part load had the laminar flame speed of the butanol blends calculated using coefficients tuned for gasoline (Scala et al., 2016). For the calibration of a quasi-dimensional model of engines operating with hydrogen and methanol plus hydrogen addition, tuning constants for the turbulent velocity model and the eddy burn time model were optimized based on experimental investigations (Ji et al., 2016; Kéromnès et al., 2014). In any case, whether zero-dimensional or quasi-dimensional, these models still require tuning of empirical correlations for specific fuels and engines. Generally, the two main engine output parameters compared during the tuning process are the combustion phasing and indicated mean effective pressure (Kéromnès et al., 2014).

Combustion phasing is a key parameter for engine performance. For a given engine, fuel and operating condition, there is a minimum spark advance for best torque (MBT), that is, the minimum spark timing advance at which the engine produces the maximum brake torque output (Heywood, 2018). Once mass fraction burned and pressure curves are strongly related (Heywood, 2018), for a given MBT timing one can define a corresponding combustion phase indicator. The most widely used are the crank angle for the peak cylinder pressure (CA_{pp}) and a corresponding crank angle for the consumption of 50% of the fuel mass (CA_{50}), and these parameters vary depending on the design and operating variables (Caton, 2014). In conventional engines, these values usually range between 9 and 16° ATDC for CA_{pp}, and between 5 and 11° ATDC for CA_{50} (Heywood, 2018; Zhu et al., 2003a; Machado et al., 2015; Caton, 2014; Ayala et al., 2006; Carvalho et al., 2012; Ravaglioli et al., 2011; Ponti et al., 2010; Lavoie et al., 2013; Zhu et al., 2006). For high efficiency engines (high dilution, high compression ratio (Caton, 2014), the optimum values are between 2 and 7° ATDC for CA_{50} and CA_{pp} around 8 °ATDC (Caton, 2014). In addition to the engine operating characteristics, fuel properties can affect combustion phasing: the higher the flame propagation speed, the faster the combustion process, thus causing a shift in CA_{50} (Machado et al., 2015). The use of CA_{pp} adjustment is reported as a better option than CA_{50} for spark timing and combustion phasing control (Gong et al., 2020).

With regard to the engine virtual calibration, it is desirable to have a relatively simple simulation model that can accurately predict the engine performance parameters without manual tuning of the combustion model parameters when used with different fuels, engine configurations, and operating conditions. One way of achieving that is by making sure the main parameters in the combustion model vary with the main variables characterizing engine operating conditions (Giglio and di Gaeta, 2020). This can be done by fitting data and correlating engine operating variables

with the model parameters and combustion phenomena (de Faria et al., 2017; Giglio and di Gaeta, 2020; Gutiérrez et al., 2020; Maroteaux and Saad, 2013; Maroteaux et al., 2015; Sun et al., 2017; Babajimopoulos et al., 2009; Vàvra and Takáts, 2004; Lindström et al., 2005; Galindo et al., 2011; Grajales et al., 2016). This approach was used to develop an enhanced Wiebe-based combustion model that has the same predictive ability as a turbulent entrainment combustion model (Giglio and di Gaeta, 2020). In a zero-dimensional thermodynamic model developed to predict the performance of a turbocharged diesel engine converted to operate lean in spark ignition mode with natural gas, correlations created to estimate the Wiebe parameters and combustion efficiency showed errors of less than 5% (Gutiérrez et al., 2020). Using a similar approach as Babajimopoulos et al. (2009), the laminar flame propagation speed, turbulent operation, and Wiebe combustion parameters were correlated (Lindström et al., 2005). The MBT spark timing was shown to correlate strongly to the maximum rate of pressure change and be related to CA_{pp} and CA_{50} to develop a closed-loop MBT timing control (Zhu et al., 2003b).

The model parameters to be tuned are the decision variables in the set up of an optimization problem, where one or more output metrics of interest (i.e. combustion phasing or engine power output) are the objective functions (Kéromnès et al., 2014; Cocco Mariani et al., 2019; Guardiola et al., 2018; Benedetto et al., 2015). CA_{50} and *IMEP* have previously been used as objective functions in the calibration of a Diesel engine (Benedetto et al., 2015), in a similar approach to the one used in this paper.

At any rate, these tuning procedures, correlations, and optimizations seldom include simultaneous calibration of the heat transfer parameters. According to Refs. Brunt and Platts (1999) and Caton (2012), improper representation of the heat transfer factors results in less accuracy of net heat release rate prediction. This can explain why, despite the accurate prediction of MFB, the pressure curve prediction was not as good when using quasi-dimensional models (Pashaei and Khoshbakhti Saray, 2019; Mehra et al., 2018), or when using optimization to calibrate Wiebe models (Rocha, 2016). According to Carvalho et al. (2012), combustion phasing for MBT timing is strongly dependent on the wall heat transfer. Thus, in addition to the combustion model parameters to be tuned, it is crucial to include the heat transfer model parameters in the decision variables.

With respect to the previous works, the novelties introduced in this work are represented by: (i) the considered set of parameters, that is the load parameter and the choice of peak pressure point (CA_{pp}) for combustion phasing; (ii) the addition of heat transfer parameters to the variables to be tuned, which usually consists only of the combustion model parameters. This is done so the net heat release rate is calculated for the target work output for a given combustion phasing; (iii) a comparison between Wiebe and Fractal combustion models ; (iv) validation of the auto-calibration methodology for a range of operating conditions, engines, and alternative fuels, namely ethanol, hydrogen and natural gas.

Based on known engine and fuel data, a corresponding model was developed on a simulation software. Then, an optimization problem was defined, where the objective functions were the indicated mean effective pressure in the high-pressure cycle (*IMEPHP)* and CA_{pp}. *IMEPHP* and CA_{pp} were chosen to represent engine load and combustion phasing, respectively. The decision variables chosen were the combustion and heat transfer model parameters. The appropriate constraints were included to guarantee that the engine model was representative of the physical problem. The method was validated with the experimental results of different engines operating in various operating conditions and using alternative fuels, namely ethanol, natural gas and hydrogen. Finally, *IMEPHP, CA_{pp}* and pressure curve were compared for all cases and CA_{10}, CA_{50} and CA_{90} when available. In particular, two cases were simulated using the same experimental data applied before for predictive simulation (Gutiérrez et al., 2020), but with a different approach for the simulation method, namely the inclusion of heat transfer factors in the optimization procedure.

2. Model description

The commercial software AVL Boost® was used to simulate the engine cycle in this research. The full description of the equations and models implemented can be found in AVL (2019a). However, to better understand the relationships of the parameters of interest, the main mathematical equations and assumptions are presented in this section.

2.1. Thermodynamic model description

Fig. 1 shows the energy balance in the cylinder modeled in AVL Boost this paper where $p_c dV$ is the work done by the piston, dQ_W is the wall heat loss rate, $h_{BB}dm_{BB}$ is the enthalpy flow due to blow-by, m_c is the mass inside the cylinder, p_c is the cylinder pressure, T_c is the cylinder temperature, V is the cylinder volume, $h_i dm_i$ is the enthalpy flow into the cylinder, and $h_e dm_e$ is the enthalpy flow out of the cylinder. Eq. (1) shows the conservation of energy and calculation of the rate of change of internal energy as a function of crankshaft angle (AVL, 2019a):

$$\frac{d(m_c u)}{d\alpha} = \sum \frac{dm_i}{d\alpha} h_i - \sum \frac{dm_e}{d\alpha} h_e - p_c \frac{dV}{d\alpha} + \frac{dQ_F}{d\alpha} - \sum \frac{dQ_W}{d\alpha} - h_{BB} \frac{dm_{BB}}{d\alpha} \quad (1)$$

where $\frac{d(m_c u)}{d\alpha}$ is the rate of change of internal energy in the cylinder (kJ/ °CA); $-p_c \frac{dV}{d\alpha}$ is the work done by the piston (kJ/ °CA); $\frac{dQ_F}{d\alpha}$ is the fuel heat release rate (kJ/ °CA); $\sum \frac{dQ_W}{d\alpha}$ is the wall heat loss rate (kJ/ °CA); $h_{BB} \frac{dm_{BB}}{d\alpha}$ is the enthalpy flow due to blow-by (kJ/ °CA); m_c is the mass inside the cylinder (kg); u is the specific internal energy (kJ/kg); p_c is the cylinder pressure (kPa); T_c is the cylinder temperature (K); V is the cylinder volume (m^3); Q_F is the heat released by the fuel (kJ); Q_W is the heat lost to the walls (kJ); α is the crank angle (°CA); and h_{BB} is the blow-by gas specific enthalpy (kJ/kg).

Eq. (1) adopts the following simplifications:

- The mixture is homogeneous at the beginning of combustion
- The air–fuel ratio of the unburned mixture is constant during combustion
- Burnt and unburnt gases have the same pressure and temperature but have different compositions
- No fuel evaporation inside the cylinder.

Eq. (2) presents the conservation of mass and calculates the mass variation inside the cylinder from the mass input and output flows (AVL, 2019a):

$$\frac{dm_c}{d\alpha} = \sum \frac{dm_i}{d\alpha} - \sum \frac{dm_e}{d\alpha} - \frac{dm_{BB}}{d\alpha} \quad (2)$$

where $\frac{dm_c}{d\alpha}$ is the in-cylinder mass flow rate (kg/ °CA); $\sum \frac{dm_i}{d\alpha}$ is the mass flow into the cylinder (kg/ °CA); $\sum \frac{dm_e}{d\alpha}$ is the mass flow out of the cylinder (kg/ °CA); and $\frac{dm_{BB}}{d\alpha}$ is the blow-by mass flow rate (kg/ °CA).

Eq. (3) shows the ideal gas equation, which relates the pressure with volume, mass and temperature through the universal gas constant (R_0) (Melo, 2012; Cocco Mariani et al., 2019).

$$p_c = \frac{1}{V} m_c R_o T_c \quad (3)$$

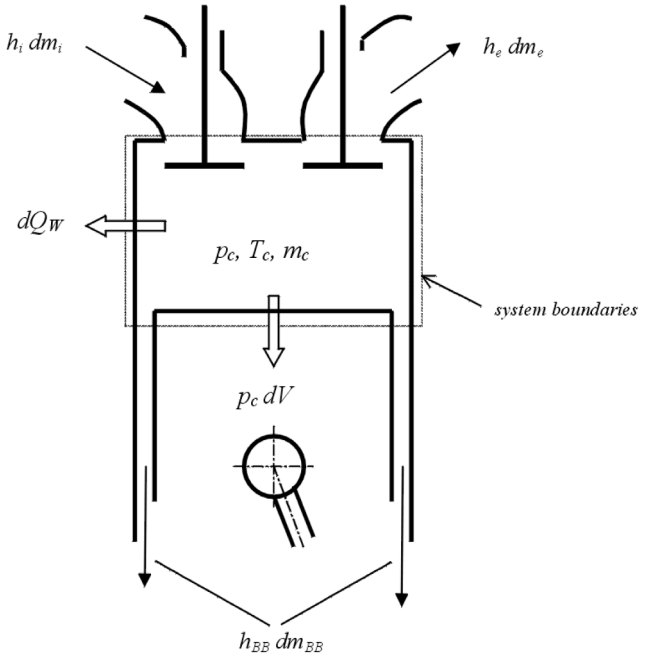

Fig. 1. Energy balance applied to the cylinder gas content (AVL, 2019a).

Then, applying the Runge–Kutta method, one can solve for the temperature using Eqs. (1) to (3). Given the temperature of the gases in the cylinder, the ideal gas equation provides the pressure inside the cylinder (Melo, 2012; Cocco Mariani et al., 2019; Guardiola et al., 2018; Benedetto et al., 2015).

When considering only the high-pressure cycle, the period between intake valve closing and exhaust valve opening, it is possible to simplify Eq. (1) as:

$$\frac{d(m_c u)}{d\alpha} = -p_c \frac{dV}{d\alpha} + \frac{dQ_{Net}}{d\alpha} \tag{4}$$

The term $\frac{dQ_{Net}}{d\alpha}$ in the right-hand side of Eq. (4) corresponds to the net heat release rate term and is given by:

$$\frac{dQ_{Net}}{d\alpha} = \frac{dQ_F}{d\alpha} - \sum \frac{dQ_W}{d\alpha} - h_{BB}\frac{dm_{BB}}{d\alpha} \tag{5}$$

In Eq. (4), the term $-p_c \frac{dV}{d\alpha}$ is the work done by the piston. Integrating this term, the indicated mean effective pressure of the engine, *IMEP* (kPa), is defined as:

$$IMEP = \frac{\oint p_c dV_\alpha}{V_d} \tag{6}$$

where V_d is the displacement volume (m^3).

The high-pressure cycle IMEP, *IMEPHP*, is given by:

$$IMEPHP = \frac{\int_{\alpha_{IVC}}^{\alpha_{EVO}} p_c dV_\alpha}{V_d} \tag{7}$$

With an adequate engine friction model and the intake and exhaust processes, it could be possible to relate the piston work to the brake power. However, as this is not in the scope of this work, *IMEPHP* is here used as a load parameter.

The net heat release rate is a function of fuel heat release rate, heat transfer and blow-by enthalpy. The fuel heat release rate term $\frac{dQ_F}{d\alpha}$ is given by:

$$\frac{dQ_F(\alpha)}{d\alpha} = m_f LHV_F \frac{dx(\alpha)}{d\alpha} \tag{8}$$

where m_F is the fuel mass (kg), LHV_F is the fuel lower heating value (kJ/kg) and $\frac{dx(\alpha)}{d\alpha}$ is the burn rate (kJ/°CA).

The burn rate is related to the mass fraction burned, which is also related to combustion phasing. Here, CA_{pp} is used as a definition for combustion phasing, which, according to Gong et al. (2020), is a better option than CA_{50} for spark timing and combustion phasing control.

This paper uses two-zone combustion models (Cocco Mariani et al., 2019; AVL, 2019a; BUENO, 2016), where the control volume is split into two zones and the first law of thermodynamics is applied to the burned and unburned zones, separately, considering different temperatures in the burned and unburned gases. This principle is applied when both valves are closed, while in the open part of the engine operation cycle, Eq. (1) still applies:

(i) Wiebe combustion model (Vibe and Meizner, 1970) – 0D model with four tuning parameters; and
(ii) Fractal geometry model (North and Santavicca, 1990) – quasi-dimensional model with seven tuning parameters and requires detailed combustion chamber geometry.

A brief discussion of these two models and their tuning parameters follows. The interested reader is referred to AVL (2019a) for more details on implementation and Refs. Vibe and Meizner (1970) for a more in-depth discussion of the Wiebe and Fractal geometry combustion models, respectively.

Wiebe combustion model

Wiebe equation is a widely known empirical equation and has been used in engine modeling research for different fuels such diesel (BUENO, 2016; Souza Junior, 2009), gasoline (Melo, 2012; AVL, 2019a; Caton, 2016), or natural gas and biofuels such as biogas, ethanol, biodiesel, hydrogen and their blends using these models (Shivapuji and Dasappa, 2017; de Faria et al., 2017; Melo, 2007, 2012; Yeliana et al., 2011; Rocha, 2016; Reyes et al., 2013, 2016). Its equation calculates the fuel mass fraction burned ($x(\alpha)$) as follows:

$$x(\alpha) = 1 - e^{-a_{wiebe}\left(\frac{\alpha-\alpha_i}{\Delta\alpha}\right)^{m_{wiebe}+1}} \tag{9}$$

where the four tuning constants are: coefficient a, which is normally used to model spark plug number and location; coefficient m_{wiebe}, known as combustion chamber shape factor and models the propagation flame front; α_i, the start of energy release or start of combustion; and $\Delta\alpha$, the combustion duration.

Fractal geometry model

The fractal geometry model for spark ignition engines is used to calculate the mass burning rate and falls in the wrinkled-corrugated flamelet zones reported in the well-known Borghi diagram (De Bellis et al., 2017). This model can predict the heat release rate of a homogeneous charge provided the following are known (AVL, 2019a):

- Combustion chamber geometry;
- The spark plug location and spark timing;
- The composition of the cylinder charge (air, fuel vapor, residuals, recirculated exhaust gas *etc.*);
- Macroscopic charge motion and turbulence level.

An initial smooth and spherical, thin flame surface centered in the spark plug location with laminar flame front surface area (A_L) is wrinkled due to the interaction with turbulent eddies. The interactions between the turbulent flow field and the flame determine the development of the turbulent surface area (A_T), which is much larger than A_L due to the wrinkling and propagates at the laminar flame speed (S_L) (AVL, 2019a). Assuming a self-similar wrinkling within the length scale intervals ($L_{min} - L_{max}$), then the flame will present the characteristics of a fractal object. AVL (2019a) states that the increase in the flame surface (A_T/A_L) is the most influential factor with respect to the increase of

combustion rate when compared with the laminar propagating flame. The burning rate is computed using the turbulent burning speed (S_T), increase in the flame area, laminar flame surface, and unburned gas density (ρ_u) (Damköhler, 1940). Thus, the burning rate can be given as (AVL, 2019a):

$$\frac{dm_b}{dt} = \rho_u A_T S_T = \rho_u \left(\frac{A_T}{A_L}\right) A_L S_L with \left(\frac{S_T}{S_L}\right) = \left(\frac{A_T}{A_L}\right) \quad (10)$$

As previously mentioned, the full description of the fractal geometry model falls outside the scope of this paper. However, the 7 tuning constants and how they relate to the model are presented. The interested reader is referred to AVL (2019a) for more details. The first tunable constant is the residual gas content influence parameter which adapts the laminar flame speed (S_T) depending on the residual gas mass fraction in the cylinder.

The turbulence model used in this work is a standard *K-k* approach (AVL, 2019a; Poulos and Heywood, 1983). There is a tuning constant of order 1 (c_t) that affects the turbulent production term that characterizes the energy transfer between the mean and the turbulent flow-fields using the energy-cascade mechanism (Poulos and Heywood, 1983). Under the assumption of isotropic turbulence, it is possible to use the standard *K-k* model to calculate the Kolmogorov length scales, which represent the maximum and minimum wrinkling scales. These length scales can be tuned with parameter c_l, which is a proportional constant, ranging between 0.2 and 0.9. The turbulence–combustion interaction parameter ($m_{fractal}$) is used to tune the turbulence by adapting the maximum length scale. According to AVL (2019a), this model is valid for a fully-developed and freely expanding turbulent flame. However, this model requires weight factors to correct the modeled behavior during both early flame development and combustion completion.

The ignition process and flame kernel evolution are described in detail elsewhere (Herweg and Maly, 1992). The flame wrinkling process starts after the end of the kernel initiation process with a stable and spherically-shaped smooth flame of about 2 mm radius. The wrinkling rate depends on the turbulent intensity, which is proportional to engine speed, and the instantaneous flame radius. The kernel initiation process is tuned with the ignition-formation multiplier (c_{ign}) while the non-dimensional wrinkling rate can be calibrated using parameter $r_{f,ref}$, which is a tunable reference radius of order 1 cm.

When the flame front reaches the combustion chamber walls, the fractal model described is no longer valid. Thus, the most important characteristics of the combustion completion are the effects of the wall on the burning, due to changes in the fundamental behavior of the combustion compared with the freely propagating flame (AVL, 2019a; Bozza et al., 2001). From 30% to 40% of the unburned mixture is burned this way. The wall-combustion rate is described by (AVL, 2019a):

$$\left(\frac{dm_b}{dt}\right)_{wall-combustion} = \frac{m - m_b}{\tau} \quad (11)$$

where τ is the characteristic time scale of the wall-combustion process.

Thus, the mass burning rate is described as the weighted mean between the fractal combustion and the wall-combustion processes. The tunable parameter $w_{fractal}$ is the mass fraction burned at which the wall-combustion process begins (AVL, 2019a).

Heat transfer model

According to Caton (2014), combustion phasing is mostly influenced by the heat transfer level. This highlights the importance of the $-\sum \frac{dQ_W}{d\alpha}$ term. Part of the novelty of this method is the inclusion of the heat transfer term as part of the tuning. Eq. (12) is used to calculate the heat transfer to the cylinder walls (head, piston and cylinder liner) (AVL, 2019a,b):

$$Q_w = \sum_{i=1}^{3} A_{w,i}(\alpha)\, h_w(\alpha) \left(T_c(\alpha) - T_{w,i}\right) \quad (12)$$

where $i = 1$, 2, and 3 represent the cylinder walls (cylinder liner, piston, and head surfaces respectively); $A_{w,i}(\alpha)$ is the combustion chamber surface area (m^2); T_{wi} is the cylinder wall temperature (K); $h_w(\alpha)$ is the heat transfer coefficient (W/m^2K); and $T_c(\alpha)$ is the bulk gas temperature inside the cylinder (K).

The heat transfer coefficient h_w is calculated using Bargende's model (AVL, 2019a; Bargende, 1991). This model has the following tuning parameters:

- $htm_{Wpiston}$, htm_{Whead}, and htm_{Wliner}, which are the piston, cylinder head, and cylinder liner wall heat transfer multipliers, respectively;
- $T_{Wpiston}$, T_{Whead}, $T_{WlinerTDC}$, and $T_{WlinerBDC}$, which are the temperatures of the piston crown, cylinder head, cylinder liner at top dead center (TDC) crank position, and cylinder liner at bottom dead center (BDC) crank position, respectively.

In the first set of validation cases, the heat transfer tuning parameters and temperature values were used by default. The other cases, however, had these tuning parameters and temperatures as decision variables of the optimization procedure.

Blow-by model

Finally, the enthalpy flow due to blow-by, $-h_{BB}\frac{dm_{BB}}{d\alpha}$, depends on the effective blow-by gap (δ_{BBY}) and is determined as detailed by AVL (2019a). In the first set of validation cases, "typical" values were chosen for the heat transfer rate. According to Brunt and Platts (1999), this results in small errors in calculating the net heat release rate. Thus, the blow-by losses were used as a correction factor for the net heat release rate. The tuning parameter varied in this case is the effective cylinder blow-by gap. Although not physically accurate, as the blow-by gap would not vary, the trends verified are still qualitatively crucial. It is representative of in-cylinder losses and their influence on in-cylinder pressure. In all other cases, the blow-by gap was fixed at the default value of 0.0008 mm.

2.2. Optimization method

Multi-objective optimization is an interesting approach for combustion parameter tuning, increasing the efficiency by relieving the operator from the decision-making process. The general definition of multi-objective optimization is as follows:

Minimize $|\boldsymbol{U}(\boldsymbol{x})_{\boldsymbol{desired}} - \boldsymbol{U}(\boldsymbol{x})_{\boldsymbol{simulated}}|$

Subject to:

$\boldsymbol{c}(\boldsymbol{x}) = 0$

$\boldsymbol{g}(\boldsymbol{x})_{\boldsymbol{lb}} \leq \boldsymbol{g}(\boldsymbol{x}) \leq \boldsymbol{g}(\boldsymbol{x})_{\boldsymbol{ub}}$

$\boldsymbol{x}_{\boldsymbol{lb}} \leq \boldsymbol{x} \leq \boldsymbol{x}_{\boldsymbol{ub}}$

where:

$\boldsymbol{x} \in R^n$: vector of unknown variables

$\boldsymbol{U}(\boldsymbol{x})_{\boldsymbol{desired}} \in R^l$: vector of the target values of the objective functions

$\boldsymbol{U}(\boldsymbol{x})_{\boldsymbol{simulated}} \in R^l$: vector of the values of the objective functions obtained through simulation

$\boldsymbol{c}(\boldsymbol{x}) \in R^m$: vector of equality constraint equations

$\boldsymbol{g}(\boldsymbol{x}) \in R^n$: vector of inequality constraint equations

$\boldsymbol{g}(\boldsymbol{x})_{\boldsymbol{lb}} \in R^n$: vector of lower bound values of $\boldsymbol{g}(\boldsymbol{x})$

$\boldsymbol{g}(\boldsymbol{x})_{\boldsymbol{ub}} \in R^n$: vector of upper bound values of $\boldsymbol{g}(\boldsymbol{x})$

$\boldsymbol{x}_{\boldsymbol{lb}} \in R^o$: vector of lower bound values of $\boldsymbol{x}$

$\boldsymbol{x}_{\boldsymbol{ub}} \in R^o$: vector of upper bound values of $\boldsymbol{x}$

l : number of objective functions

m : number of equality constraints

n : number of unknown variables
o : number of inequality constraints

The current work uses a multi-objective genetic algorithm (MOGA) method to estimate the combustion and heat transfer parameters required to minimize the difference between the target and the objective function simulated values. In this case, the objective functions are *IMEPHP* and CA_{pp}. The MOGA implementation has been adapted to deal with multi-objective optimization problems and uses a non-dominated ranking and selection scheme to compute an individual's efficiency. In each generation, the nearest individuals to the optimal results are used to produce the next population. Further explanation of the multi-objective genetic algorithm can be found in AVL (2019c).

3. Materials and method

This section elaborates on the methods used in this paper, first presenting the software tools used then following with an explanation of the simulation procedure. The result metrics that will be compared with experimental data for validation are discussed, and the validation cases introduced.

3.1. Materials

The proposed method consists of two parts: the simulation of the internal combustion engine and the optimization procedure to tune the decision variables. The AVL Boost software (AVL, 2019b) is used for engine cycle simulation and the AVL Design Explorer software (AVL, 2019c) is applied for the optimization. The decision variables from the optimization problem are varied in AVL Design Explorer and provide inputs to the AVL Boost model. The AVL Boost output is then returned to AVL Design Explorer for objective function evaluation until the evaluation process is finished.

3.2. Methodology

This sub-section details the method used in this paper, introducing the decision variables that are optimized with AVL Design Explorer and the ranges of values chosen. Then, the constraints of the optimization problem are presented, together with the definition of the objective functions aimed to be minimized and the optimization parameters, followed by the simulation procedure.

3.2.1. Design variables

As previously explained, the parameters of the combustion and heat transfer models are tuned to adjust the net heat release rate. To this end, these tuned parameters are the decision or design variables of the optimization problem. For the combustion model, either the fractal geometry or Wiebe model is used. Tables 1 and 2 show a description of the parameters involved in the fractal geometry model and Wiebe model, respectively. Table 3 presents a description of the heat transfer parameters (Cocco Mariani et al., 2019; de Cristo, 2017; Vibe and Meizner, 1970; Souza Junior, 2009). When relevant, the effective blow-by gap, δ_{BB}, is used as a design variable while the heat transfer model parameters are fixed, otherwise the opposite happens.

Finally, Table 4 shows the lower and upper limits of the decision variables (Cocco Mariani et al., 2019; Vibe and Meizner, 1970; Caton, 2016; Damköhler, 1940).

3.2.2. Constraints

One novelty of this method is the inclusion of the heat transfer parameters as decision variables for the optimization problem concurrently with the combustion model parameters. However, the temperature profile in the cylinder needs to be constrained so that the simulation model is realistic. Thus, cylinder temperatures constraints are used based on empirical observations of a wide range of engines (Prah et al., 2016). Furthermore, another constraint is set to guarantee that CA_{pp} happens after CA_{50}. Table 5 lists the constraints applied and their lower and upper boundaries.

3.2.3. Objective functions

The objective functions to be minimized are defined as:

$$|IMEP - HP_{desired} - IMEP - HP_{simulated}|$$
$$\left|CA_{pp\,desired} - CA_{pp\,simulated}\right|$$

3.2.4. Optimization parameters

For the optimization problem, the MOGA algorithm parameters are set in AVL Design Explorer (AVL, 2019c) as shown in Table 6. The mutation probability is set as $\frac{1}{n}$, where n is the number of decision variables (Deb et al., 2002) and the other values are a combination of recommended values and empirical ones (AVL, 2019c).

3.2.5. Solution procedure overview

Fig. 2 shows a flowchart detailing the steps involved in this method. It begins by defining the engine, fuel and operating case. Then, using AVL BOOST, the simulation model that represents the engine is built. The combustion and heat transfer models will be used are defined and parametrized so that these can become design variables in Design Explorer during the optimization process. The next step is to enter the operating case input data, such as equivalence ratio, engine speed, intake manifold pressure, and fuel and air mass flow rates. The final step using AVL Boost is defining the model responses, such as *IMEPHP*, CA_{pp}, and other output metrics that are discussed in the next section.

Next, the optimization problem on AVL Design Explorer is defined through the objective functions, design variables, and constraints. Afterwards, the optimization problem is solved and the results compared with the ones obtained experimentally. If there is another case to simulate it returns to the engine and operating case definition, otherwise the process is ended.

3.3. Output metrics

The first output metrics compared with experimental results are *IMEPHP* and CA_{pp}. Also, CA_{10}, CA_{50} and CA_{90} are compared as an indicator of the mass fraction burned behavior, and the maximum in-cylinder peak pressure (P_{max}). The main intention to present these MFB metrics is to verify if it is possible to predict CA_{50} when using CA_{pp} as combustion phasing indicator. Furthermore, CA_{10} and CA_{90} are included to discuss how well the models predict the combustion phenomena.

Furthermore, the predicted in-cylinder pressure curves are compared to the experimental results. The simulated curve is recorded between −150 °CA ATDC and 150 °CA ATDC at 1 °CA intervals. Due to the different sources of the measured in-cylinder pressure, the corresponding curves needed to be normalized. Thus, these curves were interpolated using WebPlotDigitizer (Rohatgi, 2020) and the points between −150 °CA ATDC and 150 °CA ATDC were extracted at 1 °CA intervals. Then, the measured and predicted datasets were used to calculate the coefficient of

determination R^2, shown in Eq. (13), **w**hich is taken as a measure of fit adequacy.

$$R^2 = \left[\frac{\sum \left(p_{exp} - \overline{p_{exp}}\right)\left(p_{sim} - \overline{p_{sim}}\right)}{\sum \left(p_{exp} - \overline{p_{exp}}\right)^2 \sum \left(p_{sim} - \overline{p_{sim}}\right)^2} \right]^2 \quad (13)$$

where p_{sim} is the point in the simulated pressure curve (kPa); p_{exp} is the point in the experimentally measured pressure curve (kPa); $\overline{p_{sim}}$ is the mean of the values of all points in the simulated pressure curve (kPa), and $\overline{p_{exp}}$ is the mean of the values of all points in the experimentally measured pressure curve (kPa).

3.4. Validation cases

In order to verify the utilization of the method in a range of operating conditions, engines and fuels, three different engine data found in the literature were used to validate the method, representing three major case sets (Moreira, 2018; de Morais et al., 2019; de Almeida et al., 2015; Gutiérrez, 2011):

- Set I – MWM D229-4 – 3.922 L, naturally aspirated diesel engine converted to operate with ethanol (EHC) at 1800 RPM (Moreira, 2018; de Morais et al., 2019) ;
- Set II – Fiat Fire 1.0 – 1.0 L, naturally aspirated flex-fuel spark ignition engine operating with ethanol and modified to run with ($EHCH_2$) or without (EHC) hydrogen addition at 1400 RPM (de Almeida et al., 2015);
- Set III – Scania DC-12 – 11.7 L, turbo-charged diesel engine converted to operate with natural gas (NG) at 1800 RPM (Gutiérrez, 2011).

The pressure curves used for each case set represent the average of the in-cylinder pressure measurements of 500, 500, and 450 successive cycles for cases I, II and III, respectively, with data measured at 1 °CA interval.

For each case set, an optimization process is used to automatically calibrate the combustion model parameters and either the heat transfer model or blow-by model for a target *IMEPHP* and combustion phasing. The diversity in the set of engines, fuels and operating conditions resulted in differences on the definitions for each case set and variation of different operating parameters. The next subsections elaborate on these case sets and detail the validation cases.

3.4.1. Case Set I

In this first case set, a naturally aspirated diesel engine-generator converted to operate with ethanol fuel (Moreira, 2018; de Morais et al., 2019) was simulated using the fractal combustion model. Table 7 shows the engine data used in set I, which has a very high compression ratio and a bowl-in-piston shape. Initially, an attempt was made to obtain a solution for the optimization problem for the combustion model parameters only; however, the results were not satisfactory, as the net heat release rate was not well predicted. This is in accordance with Brunt and Platts (1999), which explains that using the "usual" heat transfer rate values results in small errors in calculating the net heat release rate.

Thus, blow-by losses were used as a "correction" factor for the net heat release rate to verify if that would improve pressure curve prediction with knowledge of combustion phasing and *IMEPHP*. However, there was high uncertainty on the measured equivalence ratio ($\lambda_{measured}$) and cylinder composition, so λ and residual gas fraction (w_{shp}) at start of high-pressure cycle are also decision variables in addition to the aforementioned parameters. The values for λ correspond to a 5% deviation from the experimentally measured values, and an upper value of 5% for residual gas fraction was found to be reasonable. Table 8 shows the lower and upper bounds of this case set. The ethanol fuel composition consists of 92.5% ethanol and 7.5% water (Moreira, 2018; de Morais et al., 2019).

Table 1
Fractal geometry combustion model parameters.

Parameter	Description
c_{ign}	Ignition delay parameter (non-dimensional)
r_{ref}	Reference flame radius (mm)
c_l	Turbulent length scale parameter (non-dimensional)
c_t	Turbulence production constant (non-dimensional)
$d_{fractal}$	Residual gas content influence parameter (non-dimensional)
$m_{fractal}$	Turbulence–combustion interaction parameter (non-dimensional)
$w_{fractal}$	Mass fraction for wall combustion (non-dimensional)

Table 2
Wiebe combustion model parameters.

Parameter	Description
α_s	Crank angle corresponding to start of combustion (°CA)
$\Delta\alpha$	combustion duration (°CA)
m_{wiebe}	combustion chamber shape factor (non-dimensional)
a_{wiebe}	Vibe parameter to model spark plug number and location (non-dimensional)

Table 3
Heat transfer model parameters.

Parameter	Description
$T_{Wpiston}$	Piston crown temperature (°C)
T_{Whead}	Cylinder head temperature (°C)
$T_{WlinerTDC}$	Cylinder liner temperature at TDC position (°C)
$T_{WlinerBDC}$	Cylinder liner temperature at BDC position (°C)
$T_{Wexhaust}$	Exhaust port temperature (°C)
$htm_{Wpiston}$	Piston wall heat transfer multiplier (non-dimensional)
htm_{Whead}	Cylinder head wall heat transfer multiplier (non-dimensional)
htm_{Wliner}	Cylinder liner wall heat transfer multiplier (non-dimensional)

Table 4
Upper and lower bound values of the design variables.

Model	Parameter	x_{lb}	x_{ub}
Fractal combustion model	c_{ign} (non-dimensional)	0	1
	r_{ref} (mm)	0.001	0.1
	c_l (non-dimensional)	0.2	0.8
	c_t (non-dimensional)	0.3162	3.162
	$d_{fractal}$ (non-dimensional)	0	15
	$m_{fractal}$ (non-dimensional)	−10	10
	$w_{fractal}$ (non-dimensional)	0.05	0.4
Wiebe combustion model	α_s (°CA)	−40	−10
	$\Delta\alpha$ (°CA)	20	180
	m_{wiebe} (non-dimensional)	0.1	2.6
	a_{wiebe} (non-dimensional)	2.303	6.908
Bargende heat transfer model	$T_{Wpiston}$ (°C)	140	290
	T_{Whead} (°C)	120	270
	$T_{WlinerTDC}$ (°C)	120	240
	$T_{WlinerBDC}$ (°C)	90	220
	$T_{Wexhaust}$ (°C)	140	270
	$htm_{Wpiston}$ (non-dimensional)	0.5	6
	htm_{Whead} (non-dimensional)	0.5	6
	htm_{Wliner} (non-dimensional)	0.5	6

Table 5
List with inequality constraint equations and their respective lower and upper bounds.

Constraint	$g(x)_{lb}$	$g(x)_{ub}$
$(T_{Wpiston} - T_{Whead})$ (°C)	15	–
$(T_{Wpiston} - T_{Wexhaust})$ (°C)	20	40
$(T_{Wpiston} - T_{WlinerTDC})$ (°C)	20	50
$(T_{Whead} - T_{Wexhaust})$ (°C)	0	–
$(T_{Wexhaust} - T_{WlinerTDC})$ (°C)	0	–
$(T_{WlinerTDC} - T_{WlinerBDC})$ (°C)	0	25
$(CA_{pp} - CA_{50})$ (°CA)	0	–

Table 6
Values for the optimization parameters.

Parameter	Value
Distribution for crossover probability (non-dimensional)	10
Distribution for crossover probability(non-dimensional)	30
Number of generations (non-dimensional)	75
Population size (individuals)	40
Crossover probability (non-dimensional)	0.9
Mutation probability (non-dimensional)	$\frac{1}{n}$

Table 7
Engine data of the MWM 229-D4 engine used in case set I.

Parameter	Description
Model	MWM 229-D4
Fuel	Ethanol (EHC)
Maximum rated power (kW)	49
Number of cylinders (non-dimensional)	4
Bore (m)	0.102
Stroke (m)	0.120
Con-rod length (m)	0.207
Compression ratio (non-dimensional)	17:1
Aspiration	Natural
Intake valve opening (°CA)	360
Intake valve closing (°CA)	570
Exhaust valve opening (°CA)	150
Exhaust valve closing (°CA)	360

Table 8
Additional decision variables for case set I.

Parameter	x_{lb}	x_{ub}
δ_{BBY} (mm)	0	0.01
λ (non-dimensional)	$95\%\lambda_{measured}$	$105\%\lambda_{measured}$
w_{shp} (%)	0	5

Table 9
Engine data of the Fiat Fire 1.0 engine used in case set II.

Parameter	Description
Model	Fiat Fire 1.0
Fuel	Ethanol (EHC) Ethanol + hydrogen produced on-board ($EHCH_2$)
Maximum rated power (kW)	55.93
Number of cylinders (non-dimensional)	4
Bore (m)	0.070
Stroke (m)	0.0649
Con-rod length (m)	0.11146
Compression ratio (non-dimensional)	12.15:1
Aspiration	Natural
Intake valve opening (°CA)	358
Intake valve closing (°CA)	573
Exhaust valve opening (°CA)	150
Exhaust valve closing (°CA)	365

Set I consists of two partial load cases:

- Case 1 – Engine operating at 20 kW and 1800 RPM with ethanol, and *IMEPHP* equal to 5.0 bar. Case simulated using fractal combustion model parameters, effective blow-by gap, w_{shp}, and λ as design variables.
- Case 2 – Engine operating at 30 kW and 1800 RPM with ethanol, and *IMEPHP* equal to 5.00 bar. Case simulated using fractal combustion model parameters, effective blow-by gap, w_{shp}, and λ as design variables.

3.4.2. Case Set II

In this second case set, a naturally aspirated flex-fuel spark ignition engine operating with ethanol and modified to run with ($EHCH_2$) or without hydrogen addition (EHC) was modeled (de Almeida et al., 2015). Table 9 shows the engine data used in set II, which is used in small passenger vehicles, and the operating

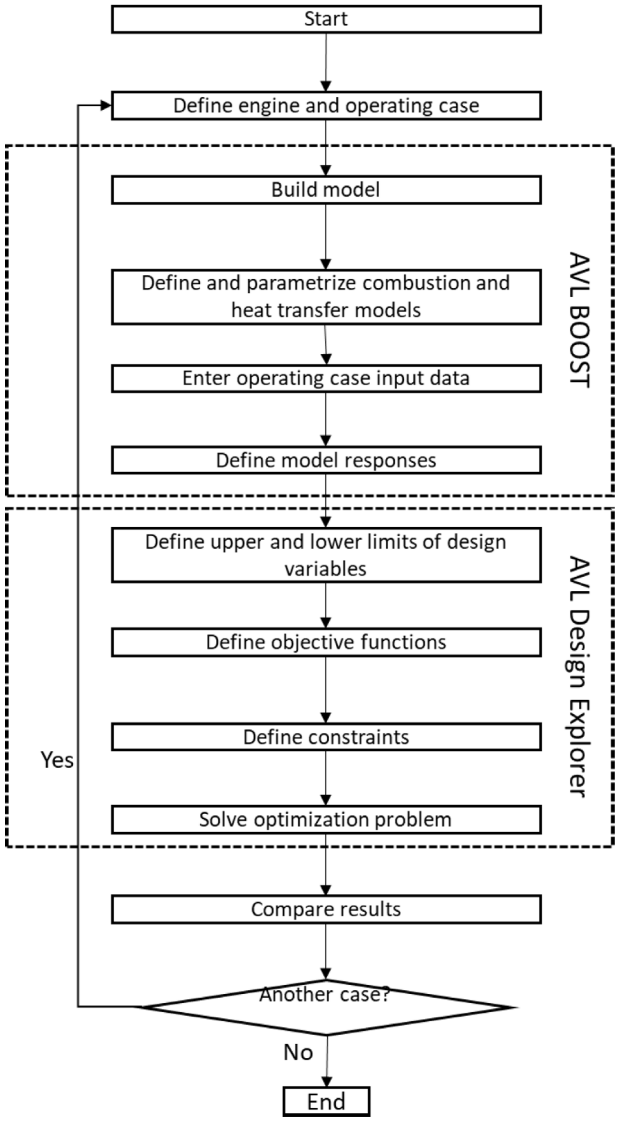

Fig. 2. Flowchart detailing the simulation steps involved in this method.

cases with varied equivalence ratio and fuel blends of ethanol and hydrogen produced on board. The main interest is to verify if the method can predict engine performance when operating with the alternative fuel mixtures at lean and stoichiometric conditions. The effective blow-by gap was fixed using default values and included heat transfer model parameters as design variables. The ethanol fuel composition is the same as the one used in case set I, consisting of 92.5% ethanol and 7.5% water. The hydrogen energy content in the hydrogen enriched ethanol mixture corresponds to 8% of the amount necessary for the engine to operate at those conditions (de Almeida et al., 2015).

Although the fractal combustion model used in case set I has the advantages of a quasi-dimensional model, it also incurs in higher computational cost, extra decision variables, and need of previous knowledge of engine combustion chamber geometry. For this engine, the exact combustion chamber geometry was not available, so the geometry of a similar engine was used (Melo, 2012; De Melo et al., 2014), which may affect the predicted results. Thus, both the fractal combustion model and the Wiebe combustion model were simulated for the same engine to validate the method with different fuel blends and equivalence ratios. To this end, two cases were simulated in this set:

Table 10
Engine data of the Scania DC-12 engine used in case set III.

Parameter	Description
Model	Scania DC-12
Fuel	Natural gas
Maximum rated power (kW)	295
Number of cylinders (non-dimensional)	6
Bore (m)	0.127
Stroke (m)	0.154
Con-rod length (m)	0.267
Compression ratio (non-dimensional)	11:1
Aspiration	Turbocharged
Intake valve opening (°CA)	360
Intake valve closing (°CA)	570
Exhaust valve opening (°CA)	150
Exhaust valve closing (°CA)	360

- Case 3 – Engine operating at 1400 RPM, part load with ethanol and hydrogen addition, λ equal to 1.0, and *IMEPHP* equal to 6.06 bar. Case simulated using fractal combustion model and heat transfer model parameters as design variables.
- Case 4 – Engine operating at 1400 RPM, part load with ethanol, λ equal to 1.07, and *IMEPHP* equal to 5.49 bar. Case simulated using Wiebe combustion model and heat transfer model parameters as design variables.

3.4.3. Case Set III

Finally, in the last case set, a lean turbo-charged diesel engine converted to operate with natural gas was modeled (Gutiérrez, 2011). As the combustion chamber geometry information is not available, only the Wiebe combustion model is used. The simulated natural gas is composed of 90.3% CH_4, 5.8% C_2H_6, 1.4% C_3H_8, 0.6% C_4H_{10}, 1.2% CO_2, and 0.7% N_2 (Gutiérrez, 2011).

Table 10 shows the engine data used in case set III, where the effective blow-by gap is fixed using default values and heat transfer model and Wiebe combustion model parameters are included as design variables. The varied parameter in this case is the engine load. Two cases are defined in this set:

- Case 5 – Engine operating with natural gas at 27% of nominal load and 1800 RPM, λ equal to 1.35, and *IMEPHP* equal to 5.73 bar. Case simulated using Wiebe combustion model and heat transfer model parameters as design variables.
- Case 6 – Engine operating with natural gas at 55% of nominal load and 1800 RPM, λ equal to 1.35, and *IMEPHP* equal to 9.91 bar. Case simulated using Wiebe combustion model and heat transfer model parameters as design variables.

3.4.4. Simulation matrix

Table 11 summarizes the cases and presents the simulation matrix used for validation.

4. Results and discussion

In this section the results and pertinent discussion are presented for application of the method outlined previously. The following output metrics obtained via simulation are compared with the available experimental data: pressure vs. crank angle curves, *IMEPHP*, CA_{pp}, P_{max}, CA_{10}, CA_{50} and CA_{90}, and R^2. The results are presented by case set for clarity, and a more general discussion of the method is included next section.

4.1. Case Set I

This case set refers to the MWM 229-D4 engine converted to operate in spark ignition mode with ethanol at different loads

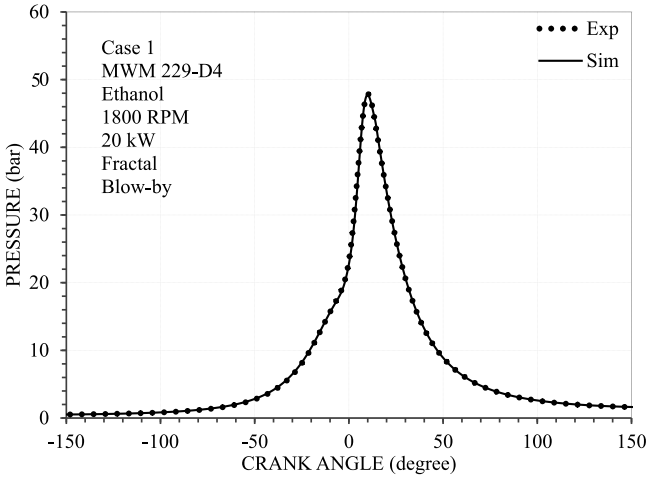

Fig. 3. Simulated (Sim) and experimental (Exp) cylinder pressure curve for case 1 using fractal combustion model and blow-by as net heat release rate correction factor.

(Moreira, 2018; de Morais et al., 2019). The fractal combustion model is used and the blow-by losses tuned to adjust the net heat release rate. Figs. 3 and 4 show the measured and predicted in-cylinder pressure curves for engine operation at 1800 RPM and two different loads, 20 kW (case 1) and 30 kW (case 2). Table 12 presents a comparison between the measured and simulated results for case set I. The predicted pressure curves closely match the experimental pressure curves, with the coefficient of determination R^2 higher than 0.99 for both cases. The results show a percentage difference of less than 2% between predicted and measured values of *IMEPHP*, CA_{pp}, and P_{max}, corresponding to very small absolute values. Furthermore, the predicted CA_{10}, CA_{50} and CA_{90} values deviated less than 0.5° from measured values for both cases. For this particular case, λ was a design variable of the optimization problem and the results found are also included in the table.

The performance results show that, as load increases from 20 kW to 30 kW and the engine operates closer to stoichiometry when approaching full load (Table 12), the equivalence ratio decreases from 1.08 to 1.03. Both CA_{pp} and CA_{50} move away from top dead center as load increases and equivalence ratio decreases. In any case, this behavior is in agreement with the values found in conventional engines, which usually range between 9° ATDC and 16° ATDC for CA_{pp}, and between 5° ATDC and 11° ATDC for CA_{50} (Heywood, 2018; Zhu et al., 2003a; Machado et al., 2015; Caton, 2014; Ayala et al., 2006; Carvalho et al., 2012; Ravaglioli et al., 2011; Ponti et al., 2010; Lavoie et al., 2013; Zhu et al., 2006).

Although the blow-by gap is a geometric parameter and should be held constant, its use as a tuning variable highlights the importance of adequate net heat release rate calibration. This is shown as the combined tuning of blow-by, combustion model parameters, and equivalence ratio produced accurate results for all output metrics, and good correlation between measured and simulated pressure curves. In particular, the MFB points matched experimental data really well, being competitive with the results found in the literature (Shivapuji and Dasappa, 2017; Mehra et al., 2018; Ma et al., 2008; Scala et al., 2016; Vancoillie et al., 2014; Verhelst et al., 2011; Ji et al., 2016). However, blow-by gap is a geometric parameter and should be held constant. Based on the previous results, the blow-by gap was fixed and the heat transfer model parameters were used for net heat release rate adjustment.

Table 11
Table indicating all the simulation cases used in this paper.

Case set	Engine	Case	Fuel	λ (non-dimensional)	Combustion model	Net heat release rate factor	IMEPHP (bar)	CA_{pp}(°CA)
I[a,b]	MWM 229-D4	1	EHC	1.08	Fractal	Blow-by	5.00	10.04
	1800 RPM	2	EHC	1.03	Fractal	Blow-by	6.70	13.92
II	Fiat Fire 1.0	3	$EHCH_2$	1	Fractal	Heat transfer	6.06	14.01
	1400 RPM	4	EHC	1.07	Wiebe	Heat transfer	5.76	12.14
III	Scania DC-12	5	NG	1.35	Wiebe	Heat transfer	5.73	7.10
	1800 RPM	6	NG	1.35	Wiebe	Heat transfer	10.14	7.52

[a] λ is a decision variable for case set I.
[b] w_{shp} is a decision variable for case set I.

Table 12
Comparison between simulation and experimental results for case set I.

Case	Parameter	Experimental	Simulated	Relative percentual difference	Absolute difference
Case 1	*IMEPHP* (bar)	5.00	4.98	0.40%	0.02
	CA_{pp} (°)	10.04	9.87	1.69%	0.17
	Peak pressure (bar)	47.86	48.09	0.48%	0.23
	CA_{10} (°)	−0.14	0.24	–	0.38
	CA_{50} (°)	5.29	5.60	–	0.31
	CA_{90} (°)	10.09	9.95	–	0.14
	R^2(non-dimensional)	0.9997		–	–
	λ (non-dimensional)	–	1.08	–	–
Case 2	*IMEPHP* (bar)	6.70	6.66	0.55%	0.04
	CA_{pp} (°)	13.92	14.04	0.86%	0.12
	Peak pressure (bar)	53.75	53.12	1.17%	0.63
	CA_{10} (°)	4.37	4.63	–	0.26
	CA_{50} (°)	9.73	10.05	–	0.32
	CA_{90} (°)	14.10	14.04	–	0.06
	R^2 (non-dimensional)	–	0.9984	–	–
	λ (non-dimensional)	–	1.03	–	–

Table 13
Comparison between simulation and experimental results for case set II.

Case	Parameter	Experimental	Simulated	Relative percentual difference	Absolute difference
Case 3	*IMEPHP* (bar)	6.06	6.05	0.17%	0.01
	CA_{pp} (°)	14.01	13.96	0.36%	0.05
	Peak pressure (bar)	34.95	34.85	0.29%	0.10
	CA_{10} (°)	−5.81	−4.19	–	1.62
	CA_{50} (°)	8.90	9.92	–	1.02
	CA_{90} (°)	28.37	30.47	–	2.10
	R^2 (non-dimensional)	–	0.9979	–	–
Case 4	*IMEPHP* (bar)	5.76	5.70	1.08%	0.06
	CA_{pp} (°)	12.14	12.15	0.08%	0.01
	Peak pressure (bar)	34.21	34.81	1.75%	0.60
	CA_{10} (°)	−8.17	−7.12	–	1.05
	CA_{50} (°)	7.90	8.05	–	0.15
	CA_{90} (°)	28.14	24.94	–	3.20
	R^2 (non-dimensional)	–	0.9994	–	–

4.2. Case Set II

Case set II refers to a naturally aspirated flex-fuel spark ignition automotive engine, model Fiat Fire 1.0, operating with both pure ethanol (EHC) and ethanol with hydrogen ($EHCH_2$) at different equivalence ratios (de Almeida et al., 2015). Both the fractal combustion model and Wiebe model are used, one for each case, and the combustion and heat transfer models tuned to adjust the net heat release rate. Two part-load operating cases were chosen, Case 3 with hydrogen enrichment at stoichiometric conditions, and Case 4 using ethanol only with equivalence ratio equal to 1.07. Case 3 and Case 4 were simulated using fractal geometry and Wiebe combustion models, respectively, and the decision variables were combustion model and heat transfer model parameters.

Figs. 5 and 6 show the measured and predicted in-cylinder pressure curves for case 3 and case 4, respectively. Table 13 presents a comparison between the measured and simulated results for case set II. Once more, the predicted pressure curves correlate well with the experimental pressure curves, with R^2 higher than 0.99 for both cases. The results show a percentage difference of less than 2% between predicted and measured values of *IMEPHP*, CA_{pp}, and P_{max} for the Wiebe model in case 4, and less than 0.5% with the fractal model in Case 3. These, however, represent small deviations in absolute values. Both CA_{pp} and CA_{50} fall in the range for conventional engines (Heywood, 2018; Zhu et al., 2003a; Machado et al., 2015; Caton, 2014; Ayala et al., 2006; Carvalho et al., 2012; Ravaglioli et al., 2011; Ponti et al., 2010; Lavoie et al., 2013; Zhu et al., 2006).

Although the fractal model was about 50% better than the Wiebe model in predicting CA_{90}, it still deviated more than Wiebe for CA_{10} and CA_{50} and was generally less accurate than the results obtained in Case Set I. These deviations in the fractal model might be due to improper modeling of the combustion chamber

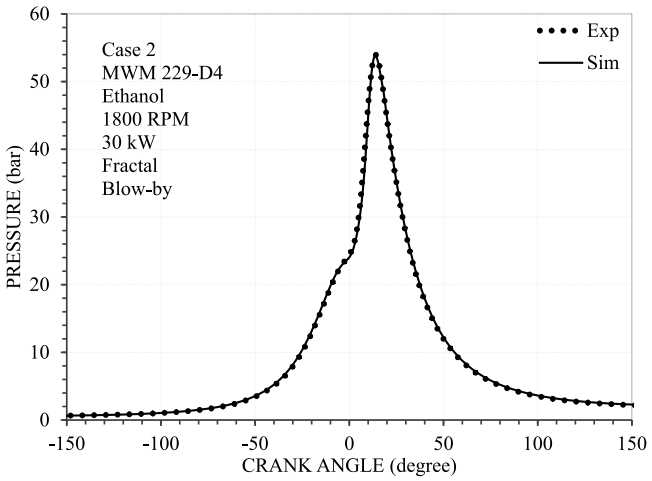

Fig. 4. Simulated (Sim) and experimental (Exp) cylinder pressure curve for case 2 using fractal combustion model and blow-by as net heat release rate correction factor.

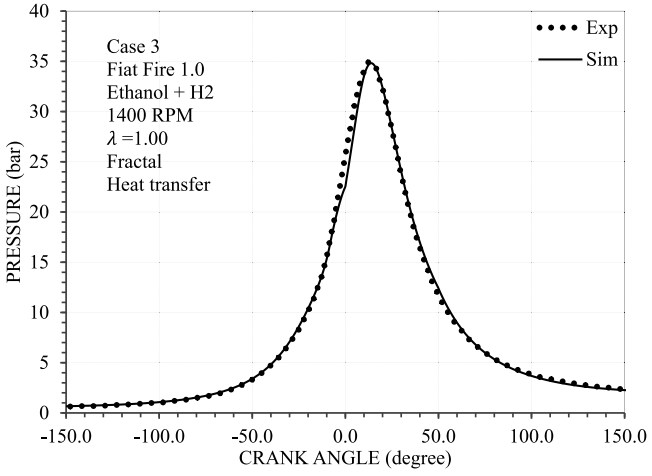

Fig. 5. Simulated (Sim) and experimental (Exp) cylinder pressure curve for case 3 using fractal combustion model and wall heat transfer as net heat release rate correction factor.

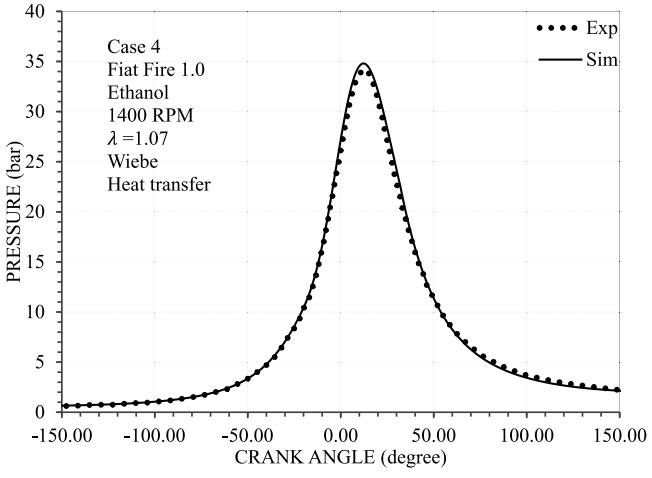

Fig. 6. Simulated (Sim) and experimental (Exp) cylinder pressure curve for case 4 using Wiebe combustion model and wall heat transfer as net heat release rate correction factor.

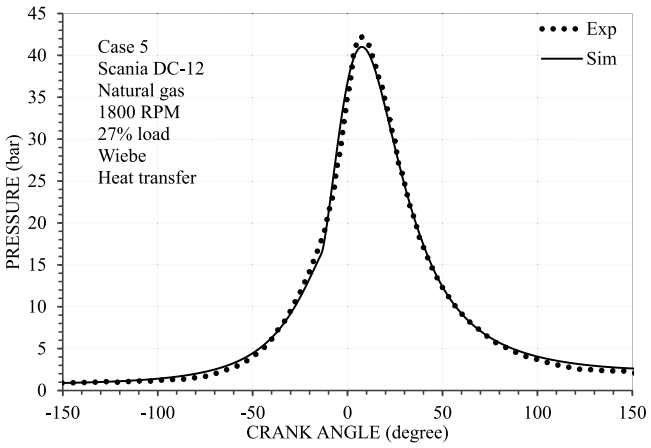

Fig. 7. Simulated (Sim) and experimental (Exp) cylinder pressure curve for case 5 using Wiebe combustion model and wall heat transfer as net heat release rate correction factor.

geometry and spark plug location. This renders this model less reliable in situations in which that data is not available. On the other hand, the Wiebe combustion model was better at predicting CA_{10} and CA_{50}, but underestimated CA_{90}.

4.3. Case Set III

Finally, in Case Set III, a lean turbo-charged diesel engine model Scania DC12 converted to operate with natural gas at different loads and lean operation at $\lambda = 1.35$ was chosen (Gutiérrez et al., 2020; Gutiérrez, 2011). Two operating cases were modeled varying engine load at 1800 RPM from 27% of nominal load in Case 5 to 55% of nominal load in Case 6. The Wiebe combustion model and heat transfer parameters were tuned to adjust the net heat release rate as design variables, as information on combustion chamber geometry was not available. The results for combustion phasing of this engine were closer to those of high efficiency engines (high dilution, high compression ratio) .

Figs. 7 and 8 show the measured and predicted in-cylinder pressure curves for case 5 and case 6. Table 14 presents a comparison between the measured and simulated results for case set III. The method successfully predicted the in-cylinder pressure curve, showing a good correlation between the measured and simulated pressure curves with R^2 higher than 0.99. The results show a percentage difference of less than 3% between predicted and measured values of *IMEPHP*, and P_{max}. Upon closer inspection, it can be noted that although CA_{pp} have error of 2%, these errors translate to less than 0.2° CA deviations. The predictive simulation was able to predict CA_{50} adequately with less than 1.5° deviation, while showing considerable deviations for CA_{10} and CA_{90} as a seemingly limitation to the use of the Wiebe model with this method.

An optimization procedure to create correlations for Wiebe parameters has been applied before to the same engine used in Case Set III, based on previous experimental results (Gutiérrez, 2011). The approach used in those works is similar to those used by other authors (de Faria et al., 2017; Giglio and di Gaeta, 2020; Maroteaux and Saad, 2013; Maroteaux et al., 2015; Sun et al., 2017; Babajimopoulos et al., 2009; Vàvra and Takáts, 2004; Lindström et al., 2005; Galindo et al., 2011; Grajales et al., 2016), correlating mass fraction burned curves, engine load and operating conditions while using Wiebe combustion parameters as decision variables. Those authors noted that the combustion efficiency in these cases was under 90% and that a fitting parameter should be included for improved prediction using Wiebe

Table 14
Comparison between simulation and experimental results for case set III.

Case	Parameter	Experimental	Simulated	Relative percentual difference	Absolute difference
Case 5	*IMEPHP* (bar)	5.7310	5.7357	0.08%	0.00
	CA_{pp} (°)	7.10	7.57	6.58%	0.47
	Peak pressure (bar)	42.05	41.02	2.46%	1.03
	CA_{10} (°)	−7.21	−9.87	–	2.66
	CA_{50} (°)	2.52	1.04	–	1.48
	CA_{90} (°)	16.66	21.72	–	5.06
	R^2(non-dimensional)	–	0.9978	–	–
Case 6	*IMEPHP* (bar)	10.1399	10.1484	0.08%	0.009
	CA_{pp} (°)	7.52	7.72	2.61%	0.20
	Peak pressure (bar)	74.20	73.90	0.41%	0.30
	CA_{10} (°)	−12.06	−15.73	–	3.67
	CA_{50} (°)	1.03	0.51	–	0.53
	CA_{90} (°)	21.86	19.67	–	2.19
	R^2(non-dimensional)	–	0.9987	–	–

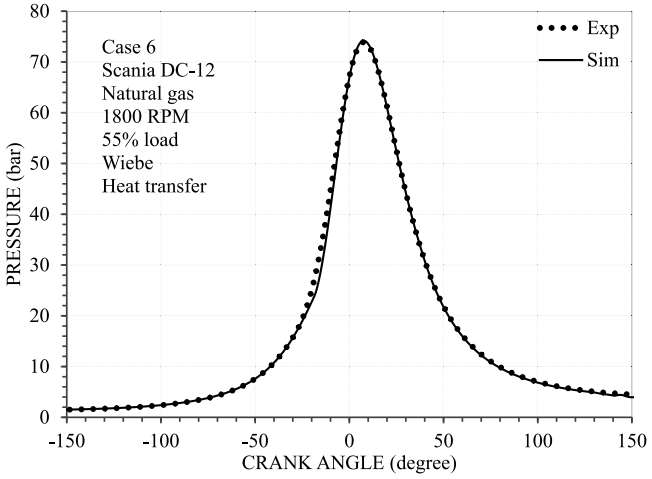

Fig. 8. Simulated (Sim) and experimental (Exp) cylinder pressure curve for case 6 using Wiebe combustion model and wall heat transfer as net heat release rate correction factor.

model (Gutiérrez, 2011). Differently from those works, only one combustion phasing point (CA_{pp}) and engine load and operating conditions have here been used as objective functions for optimization and estimation of both Wiebe combustion and heat transfer model parameters.

5. Conclusion

A novel approach to virtual engine calibration is proposed, in which a multi-objective optimization is used to tune the combustion and heat transfer model parameters to predict engine performance. The method was tested for a range of operating conditions, engines, and alternative fuels – ethanol, hydrogen and natural gas – and two different combustion models: a zero-dimensional, Wiebe model, and a quasi-dimensional, fractal geometry model. The main conclusions drawn from the results obtained are:

- This method can accurately predict *IMEPHP*, CA_{pp}, and the maximum in-cylinder peak pressure;
- The inclusion of heat transfer parameters in the decision variables contributed to accurate in-cylinder pressure curve prediction, with a coefficient of determination higher than 0.99;
- CA_{50} was well predicted independent of the combustion model, but Wiebe combustion model was not able to consistently predict CA_{10} and failed to predict CA_{90};
- When the combustion chamber geometry is known, fractal combustion model is preferred, but both models work well for general engine performance prediction.

The present method, when combined with a proper engine map, as used in engine control units, can be very useful in engine development and optimization for different fuels and operating conditions. This, in turn, can help to reduce experimental work needed and guide future engine research.

Nomenclature

ATDC	after top dead center(°CA)
BDC	bottom dead center
CFD	computational fluid dynamics
CA	crank angle (°)
CI	compression ignition
ECU	electronic control unit
EHC	ethanol
$EHCH_2$	ethanol with hydrogen addition
GHG	greenhouse gas
HIL	hardware in the loop
HRR	heat release rate (kJ/ °CA)
IMEP	indicated mean effective pressure-based (bar)
IMEPHP	indicated mean effective pressure-based in the high-pressure cycle (bar)
MBT	maximum brake torque
MFB	mass fraction burned (non-dimensional)
MOGA	multi-objective genetic algorithm
NG	natural gas
SFC	specific fuel consumption
TDC	top dead center

List of Symbols

A	area (mm^2)
$A_{w,i}$	combustion chamber surface area (mm^2)
a_{wiebe}	Wiebe parameter to model spark plug number and location (non-dimensional)
C_2H_6	ethane
C_3H_8	propane
C_4H_{10}	butane
CA_{10}	crank angle at which 10% of the fuel mass is burned (°CA)
CA_{50}	crank angle at which 50% of the fuel mass is burned (°CA)
CA_{90}	crank angle at which 90% of the fuel mass is burned (°CA)
CA_{pp}	crank angle at which the peak cylinder pressure occurs (°CA)

CH_4	methane
c_{ign}	fractal ignition delay parameter (non-dimensional)
c_l	fractal turbulent scale parameter (non-dimensional)
CO_2	carbon dioxide
c_t	fractal turbulence production constant (non-dimensional)
d_{fractal}	fractal residual gas content influence parameter (non-dimensional)
H_2	hydrogen
htm_{whead}	cylinder head wall heat transfer multiplier (non-dimensional)
htm_{wliner}	cylinder liner wall heat transfer multiplier (non-dimensional)
$htm_{wpiston}$	piston wall heat transfer multiplier (non-dimensional)
h	specific enthalpy (kJ/kg)
LHV	fuel lower heating value (kJ/kg)
m	mass (kg)
m_{fractal}	turbulence–combustion interaction parameter (non-dimensional)
m_{wiebe}	Wiebe combustion chamber shape factor (non-dimensional)
N_2	nitrogen
p_c	cylinder pressure (kPa)
p_{exp}	points in the experimentally measured pressure curve (bar)
$P_{\max}$	maximum in-cylinder peak pressure (bar)
P_{sim}	points in the simulated pressure curve (bar)
Q	heat (kJ)
R_0	universal gas constant
r_{ref}	fractal reference radius (mm)
S	burning speed (m/s)
T	temperature (K)
T_c	bulk gas temperature inside the cylinder (K)
T_{Wexhaust}	exhaust port temperature (°C)
T_{Whead}	cylinder head temperature (°C)
T_{Wi}	cylinder wall temperature (°C)
$T_{WlinerBDC}$	cylinder liner temperature at BDC position (°C)
$T_{WlinerTDC}$	cylinder liner temperature at TDC position (°C)
$T_{Wpiston}$	piston crown temperature (°C)
u	specific internal energy (kJ/kg)
$U(x)$	objective function (non-dimensional)
V	cylinder volume (m^3)
$w_{fractal}$	fractal mass fraction for wall combustion (non-dimensional)
w_{shp}	residual gas fraction (non-dimensional)
x	design variables (non-dimensional)

Greek Letters

α	crank angle (°CA)
α_s	start of combustion (°CA)
Δ	variation
δ_{BBY}	effective blow-by gap (mm)
$\Delta\alpha$	combustion duration (°CA)
λ	equivalence ratio (non-dimensional)
ρ	gas density (kg/m^3)

Subscripts

b	burning
BB	blow-by
c	cylinder
d	displacement
e	exhaust
EVO	exhaust valve opening
F	fuel
i	intake
IVC	intake valve closing
L	laminar flame surface
lb	lower boundary
max	maximum
min	minimum
T	turbulent
u	unburned
ub	upper boundary
W	wall

CRediT authorship contribution statement

Sami Massalami Mohammed Elmassalami Ayad: Conceptualization, Methodology, Investigation, Validation, Data curation, Writing - original draft. **Carolina Locatelli Vago:** Methodology, Investigation, Validation, Data curation, Writing - review & editing. **Carlos Rodrigues Pereira Belchior:** Supervision, Resources, Project administration. **José Ricardo Sodré:** Supervision, Visualization, Resources, Writing - review & editing.

Declaration of competing interest

The authors declare that they have no known competing financial interests or personal relationships that could have appeared to influence the work reported in this paper.

Acknowledgments

This study was financed in part by the Conselho Nacional de Desenvolvimento Científico e Tecnológico (CNPq), Brazil. The authors would like to thank the colleagues at the Engines, Emissions and Fuels Research Centre (CPMEC) at PUC Minas for their support and kindness.

References

AVL, 2019a. AVL BOOST Version 2019 - Theory.

AVL, 2019b. AVL BOOST Version 2019 - User Guide.

AVL, 2019c. AVL Design Explorer Version 2019 - DoE and Optimization.

Ayala, F.A., Gerty, M.D., Heywood, J.B., 2006. Effects of Combustion Phasing, Relative Air-Fuel Ratio, Compression Ratio, and Load on SI Engine Efficiency. SAE Tech. Pap., http://dx.doi.org/10.4271/2006-01-0229.

Babajimopoulos, A., Prasad Challa, V.S.S., Lavoie, G.A., Assanis, D.N., 2009. Model-based assessment of two variable cam timing strategies for HCCI engines: Recompression vs. rebreathing. In: Proc. Spring Tech. Conf. ASME Intern. Combust. Engine Div. http://dx.doi.org/10.1115/ICES2009-76103.

Bargende, M., 1991. Equations for calculating the non-steady state wall heat losses in the high pressure part of petrol engines; Ein Gleichungsansatz zur Berechnung der instationaeren Wandwaermeverluste im Hochdruckteil von Ottomotoren, Technische Hochschule Darmstadt (Germany). Fachbereich 16 - Maschinenbau.

Benedetto, M.F., Berrone, S., Scialò, S., 2015. Efficient combustion parameter prediction and performance optimization for a diesel engine with a low throughput combustion model. Energy Convers. Manag. http://dx.doi.org/10.1016/j.enconman.2015.02.071.

Bozza, F., Gimelli, A., Senatore, A., Caraceni, A., 2001. A Theoretical Comparison of Various VVA Systems for Performance and Emission Improvements of SI-Engines. SAE Tech. Pap., http://dx.doi.org/10.4271/2001-01-0670.

Brunt, M.F.J., Platts, K.C., 1999. Alculation of Heat Release in Direct Injection Diesel Engines. SAE Tech. Pap., http://dx.doi.org/10.4271/1999-01-0187.

BUENO, J., 2016. Estudo Numérico da influência das caracter{í}sticas de injeção de misturas óleo diesel-biodiesel-etanol nas emissões de nox Tese de D. Sc. COPPE/UFRJ, Rio de Janeiro, RJ, Brasil.

Carvalho, L.De O., De Melo, T.C.C., De Azevedo Cruz Neto, R.M., 2012. Investigation on the Fuel and Engine Parameters that Affect the Half Mass Fraction Burned (CA50) Optimum Crank Angle. SAE Tech. Pap., http://dx.doi.org/10.4271/2012-36-0498.

Caton, J.A., 2012. The thermodynamic characteristics of high efficiency, internal-combustion engines. Energy Convers. Manag. 58, 84–93. http://dx.doi.org/10.1016/j.enconman.2012.01.005.

Caton, J.A., 2014. Combustion phasing for maximum efficiency for conventional and high efficiency engines. Energy Convers. Manag. http://dx.doi.org/10.1016/j.enconman.2013.09.060.

Caton, J.A., 2016. An Introduction To Thermodynamic Cycle Simulations for Internal Combustion Engines. John Wiley & Sons, NY, USA.

Caton, J.A., 2018. The thermodynamics of internal combustion engines: Examples of insights. Inventions 3, 33. http://dx.doi.org/10.3390/inventions3020033.

Cocco Mariani, V., Hennings Och, S., dos Santos Coelho, L., Domingues, E., 2019. Pressure prediction of a spark ignition single cylinder engine using optimized extreme learning machine models. Appl. Energy http://dx.doi.org/10.1016/j.apenergy.2019.04.126.

Damköhler, G., 1940. Der einfluss der turbulenz auf die flammengeschwindigkeit in gasgemischen. Z. Elektrochem. Angew. Phys. Chem. 46, 601–626.

de Almeida, L.Q., Sales, L.C.M., Sodré, J.R., 2015. Fuel consumption and emissions from a vehicle operating with ethanol, gasoline and hydrogen produced onboard. Int. J. Hydrogen Energy 40, 6988–6994. http://dx.doi.org/10.1016/j.ijhydene.2015.03.167.

De Bellis, V., Bozza, F., Tufano, D., 2017. A Comparison Between Two Phenomenological Combustion Models Applied To Different SI Engines. SAE Tech. Pap. 2017, http://dx.doi.org/10.4271/2017-01-2184.

de Cristo, B.E.B., 2017. Análise dos parâmetros de desempenho de um motor de ignição por centelha operando com gasolina ou etanol com adição de hidrogênio.

de Faria, M.M.N., Vargas Machuca Bueno, J.P., Ayad, S.M.M.E., Belchior, C.R.P., 2017. Thermodynamic simulation model for predicting the performance of spark ignition engines using biogas as fuel. Energy Convers. Manag. 149, http://dx.doi.org/10.1016/j.enconman.2017.06.045.

De Melo, T.C.C., Machado, G.B., Matias, F.A.S., 2014. Using Fractal Modeling To Predict Flex-Fuel Engine Combustion Process with Different Gasoline-Ethanol Blends. SAE Tech. Pap. 2014, http://dx.doi.org/10.4271/2014-36-0162.

de Morais, A.M., de Morais Hanriot, S., de Oliveira, A., Justino, M.A.M., Valente, O.S., Sodré, J.R., 2019. An assessment of fuel consumption and emissions from a diesel power generator converted to operate with ethanol. Sustain. Energy Technol. Assess. http://dx.doi.org/10.1016/j.seta.2019.08.005.

Deb, K., Pratap, A., Agarwal, S., Meyarivan, T., 2002. A fast and elitist multiobjective genetic algorithm: NSGA-II. IEEE Trans. Evol. Comput. http://dx.doi.org/10.1109/4235.996017.

Demirbas, A., 2007. Progress and recent trends in biofuels. Prog. Energy Combust. Sci. 33, 1–18. http://dx.doi.org/10.1016/j.pecs.2006.06.001.

Demirbas, A., 2008. Biofuels sources, biofuel policy, biofuel economy and global biofuel projections. Energy Convers. Manag. 49, 2106–2116. http://dx.doi.org/10.1016/j.enconman.2008.02.020.

Galindo, J., Climent, H., Plá, B., Jiménez, V.D., 2011. Correlations for wiebe function parameters for combustion simulation in two-stroke small engines. Appl. Therm. Eng. http://dx.doi.org/10.1016/j.applthermaleng.2010.12.020.

Giglio, V., di Gaeta, A., 2020. Novel regression models for wiebe parameters aimed at 0D combustion simulation in spark ignition engines. Energy http://dx.doi.org/10.1016/j.energy.2020.118442.

Gong, C., Li, Z., Yi, L., Sun, J., Liu, F., 2020. Comparative analysis of various combustion phase control methods in a lean-burn H2/methanol fuel dual-injection engine. Fuel 262, 116592. http://dx.doi.org/10.1016/j.fuel.2019.116592.

Grajales, J.A., Quintero, H.F., Romero, C.A., Henao, E., López, J.F., Torres, D., 2016. Combustion pressure estimation method of a spark ignited combustion engine based on vibration signal processing. J. Vibroeng. 18, 4237–4247. http://dx.doi.org/10.21595/jve.2016.17311.

Grasreiner, S., 2012. Combustion modeling for virtual SI engine calibration with the help of 0D 3D methods. Tech. Univ. Bergakademie Freib. 179.

Guardiola, C., Pla, B., Bares, P., Barbier, A., 2018. A combustion phasing control-oriented model applied to an RCCI engine. IFAC-PapersOnLine http://dx.doi.org/10.1016/j.ifacol.2018.10.022.

Gutiérrez, R.H., 2011. Estudo de desempenho de um motor diesel ottolizado funcionando com gás natural através de simulação termodinâmica e análise experimental.

Gutiérrez, R.H.R., Monteiro, U.A., Vaz, L.A., 2020. Predictive thermodynamic model of the performance of a stationary spark-ignition engine running on natural gas. J. Brazilian Soc. Mech. Sci. Eng. 42, 1–16.

Herweg, R., Maly, R.R., 1992. A Fundamental Model for Flame Kernel Formation in S. I. Engines. SAE Tech. Pap., http://dx.doi.org/10.4271/922243.

Heywood, J.B., 1988. Internal Combustion Engine Fundamentals, first ed. McGraw-Hill Education, New York.

Heywood, J.B., 2018. Internal Combustion Engine Fundamentals, second ed. McGraw-Hill Education.

IEA, I., 2016a. World Energy Outlook 2016. Int. Energy Agency.

IEA, P., 2016b. CO 2 Emissions from Fuel Combustion 2016. IEA.

Isermann, R., 2014. Gasoline engine modeling and control. Mech. Eng. 137.

Jacob, A., Ashok, B., 2020. An interdisciplinary review on calibration strategies of engine management system for diverse alternative fuels in IC engine applications. Fuel 278, 118236. http://dx.doi.org/10.1016/j.fuel.2020.118236.

Ji, C., Yang, J., Liu, X., Zhang, B., Wang, S., Gao, B., 2016. A quasi-dimensional model for combustion performance prediction of an SI hydrogen-enriched methanol engine. Int. J. Hydrogen Energy http://dx.doi.org/10.1016/j.ijhydene.2016.07.146.

Kéromnès, A., Delaporte, B., Schmitz, G., Le Moyne, L., 2014. Development and validation of a 5 stroke engine for range extenders application. Energy Convers. Manag. 82, 259–267. http://dx.doi.org/10.1016/j.enconman.2014.03.025.

Lavoie, G.A., Ortiz-Soto, E., Babajimopoulos, A., Martz, J.B., Assanis, D.N., 2013. Thermodynamic sweet spot for highefficiency, dilute, boosted gasoline engines. Int. J. Engine Res. http://dx.doi.org/10.1177/1468087412455372.

Lindström, F., Angstrom, H.-E., Kalghatgi, G., Möller, C.E., 2005. An empirical {SI} combustion model using laminar burning velocity correlations. In: {SAE} Tech. Pap. Ser. {SAE} International. http://dx.doi.org/10.4271/2005-01-2106.

Ma, F., Wang, Y., Wang, M., Liu, H., Wang, J., Ding, S., Zhao, S., 2008. Development and validation of a quasi-dimensional combustion model for SI engines fuelled by HCNG with variable hydrogen fractions. Int. J. Hydrogen Energy 33, 4863–4875. http://dx.doi.org/10.1016/j.ijhydene.2008.06.068.

Machado, G.B., De Melo, T.C.C., De Mendonça Soares, L.A., 2015. Flex Fuel Engine - Influence of Fuel Composition on the CA50 At Maximum Brake Torque Condition. SAE Tech. Pap. 2015, http://dx.doi.org/10.4271/2015-36-0215.

Maroteaux, F., Saad, C., 2013. Diesel engine combustion modeling for hardware in the loop applications: Effects of ignition delay time model. Energy 57, 641–652.

Maroteaux, F., Saad, C., Aubertin, F., 2015. Development and validation of double and single Wiebe function for multi-injection mode Diesel engine combustion modelling for hardware-in-the-loop applications. Energy Convers. Manag. 105, 630–641.

Matuszewska, A., Owczuk, M., Zamojska-Jaroszewicz, A., Jakubiak-Lasocka, J., Lasocki, J., Orliński, P., 2016. Evaluation of the biological methane potential of various feedstock for the production of biogas to supply agricultural tractors. Energy Convers. Manag. 125, 309–319.

Mehra, R.K., Ma, F., Hao, D., Juknelevičius, R., 2018. Study of Turbulent Entrainment Quasi-Dimensional Combustion Model for HCNG Engines with Variable Ignition Timings. SAE Tech. Pap., http://dx.doi.org/10.4271/2018-01-1687.

Melo, T.C.C., 2007. Thermodynamic Modeling of an Otto Cycle Flexible Fuel Type Engine, Working with Gasoline, Ethanol and Natural Gas. p. 169.

Melo, T.C., 2012. Análise experimental e simulação computacional de um motor flex operando com diferentes misturas de etanol hidratado na gasolina. UFRJ, http://dx.doi.org/10.1017/CBO9781107415324.004.

Moreira, V.G., 2018. Desempenho e Emissões de Um Grupo Motor Gerador Originalmente Diesel Convertido Para Otto Operando Com Etanol. Pontifícia Universidade Católica de Minas Gerais, PUC Minas.

North, G.L., Santavicca, D.A., 1990. The fractal nature of premixed turbulent flames. Combust. Sci. Technol. http://dx.doi.org/10.1080/00102209008951648.

Pashaei, J., Khoshbakhti Saray, R., 2019. Development of a quasi-dimensional, fractal-base combustion model for SI engines by simulating flame-wall interaction phenomenon. Fuel http://dx.doi.org/10.1016/j.fuel.2018.08.155.

Ponti, F., Ravaglioli, V., Serra, G., Stola, F., 2010. Instantaneous engine speed measurement and processing for mfb50 evaluation. SAE Int. J. Engines http://dx.doi.org/10.4271/2009-01-2747.

Poulos, S.G., Heywood, J.B., 1983. The Effect of Chamber Geometry on Spark-Ignition Engine Combustion. SAE Tech. Pap., http://dx.doi.org/10.4271/830334.

Prah, I., Trenc, F., Katrašnik, T., 2016. Innovative calibration method for system level simulation models of internal combustion engines. Energies 9, 708. http://dx.doi.org/10.3390/en9090708.

Puppán, D., 2002. Environmental evaluation of biofuels. Period. Polytech. Soc. Manag. Sci. 10, 95–116.

Ravaglioli, V., Moro, D., Serra, G., Ponti, F., 2011. MFB50 on-Board Evaluation Based on a Zero-Dimensional ROHR Model. SAE Tech. Pap., http://dx.doi.org/10.4271/2011-01-1420.

Reyes, M., Melgar, A., Pérez, A., Giménez, B., 2013. Study of the cycle-to-cycle variations of an internal combustion engine fuelled with natural gas/hydrogen blends from the diagnosis of combustion pressure. Int. J. Hydrogen Energy 38, 15477–15487. http://dx.doi.org/10.1016/j.ijhydene.2013.09.071.

Reyes, M., Tinaut, F.V., Giménez, B., Pérez, A., 2015. Characterization of cycle-to-cycle variations in a natural gas spark ignition engine. Fuel http://dx.doi.org/10.1016/j.fuel.2014.09.121.

Reyes, M., Tinaut, F.V., Melgar, A., Pérez, A., 2016. Characterization of the combustion process and cycle-to-cycle variations in a spark ignition engine fuelled with natural gas/hydrogen mixtures. Int. J. Hydrogen Energy 41, 2064–2074. http://dx.doi.org/10.1016/j.ijhydene.2015.10.082.

Rocha, H.M.Z., 2016. determinação dos efeitos da utilização de hidrogênio em grupos geradores a diesel operando com diferentes misturas diesel-óleo vegetal. UFRJ/COPPE, http://dx.doi.org/10.1017/CBO9781107415324.004.

Rohatgi, A., 2020. Webplotdigitizer: Version 4.4. https://automeris.io/WebPlotDigitizer.

Scala, F., Galloni, E., Fontana, G., 2016. Numerical analysis of a downsized spark-ignition engine fueled by butanol/gasoline blends at part-load operation. Appl. Therm. Eng. http://dx.doi.org/10.1016/j.applthermaleng.2016.03.137.

Shivapuji, A.M., Dasappa, S., 2017. Quasi dimensional numerical investigation of syngas fuelled engine operation: MBT operation and parametric sensitivity analysis. Appl. Therm. Eng. http://dx.doi.org/10.1016/j.applthermaleng.2017.06.086.

Souza Junior, G.C., 2009. Simulação termodinâmica de motores diesel utilizando óleo diesel e biodiesel para verificação dos parâmetros de desempenho e emissões Dissertação de Mestrado em Engenharia Mecânica. Universidade Federal do Rio de Janeiro, RJ, p. 139.

Sun, Y., Wang, H., Yang, C., Wang, Y., 2017. Development and validation of a marine sequential turbocharging diesel engine combustion model based on double Wiebe function and partial least squares method. Energy Convers. Manag. http://dx.doi.org/10.1016/j.enconman.2017.08.085.

Tinaut, F.V., Melgar, A., Giménez, B., Reyes, M., 2011. Prediction of performance and emissions of an engine fuelled with natural gas/hydrogen blends. Int. J. Hydrogen Energy 36, 947–956. http://dx.doi.org/10.1016/j.ijhydene.2010.10.025.

Vancoillie, J., Sileghem, L., Verhelst, S., 2014. Development and validation of a quasi-dimensional model for methanol and ethanol fueled SI engines. Appl. Energy 132, 412–425. http://dx.doi.org/10.1016/j.apenergy.2014.07.046.

Vàvra, J., Takáts, M., 2004. Heat Release Regression Model for Gas Fuelled SI Engines Reprinted from : Modeling of Spark Ignition Engines. SAE Tech. Pap. 2004-01-1462.

Verhelst, S., TJoen, C., Vancoillie, J., Demuynck, J., 2011. A correlation for the laminar burning velocity for use in hydrogen spark ignition engine simulation. Int. J. Hydrogen Energy 36, 957–974. http://dx.doi.org/10.1016/j.ijhydene.2010.10.020.

Vibe, I.I., Meizner, F., 1970. Brennverlauf Und Kreisprozess Von Verbrennungsmotoren. Verlag Technik.

Xin, Q., 2011. Diesel engine system design. http://dx.doi.org/10.1533/9780857090836.

Yeliana, Y., Cooney, C., Worm, J., Michalek, D.J., Naber, J.D., 2011. Estimation of double-wiebe function parameters using least square method for burn durations of ethanol-gasoline blends in spark ignition engine over variable compression ratios and EGR levels. Appl. Therm. Eng. http://dx.doi.org/10.1016/j.applthermaleng.2011.01.040.

Yıldız, M., Çeper, B.A., 2017. Zero-dimensional single zone engine modeling of an SI engine fuelled with methane and methane-hydrogen blend using single and double Wiebe Function: A comparative study. Int. J. Hydrogen Energy 42, 25756–25765.

Zhu, G.G., Daniels, C.F., Winkelman, J., 2003a. MBT Timing Detection and Its Closed-Loop Control using in-Cylinder Pressure Signal. SAE Tech. Pap., http://dx.doi.org/10.4271/2003-01-3266.

Zhu, G.G., Daniels, C.F., Winkelman, J., 2003b. MBT Timing Detection and Its Closed-Loop Control using in-Cylinder Ionization Signal Reprinted from: SI Engine Experiment and Modeling. SAE Tech. Pap.

Zhu, G.G., Hung, D.L.S., Winkelman, J., 2006. Combustion Characteristics Detection for Low Pressure Direct Injection Engines using Ionization Signal. SAE Tech. Pap., http://dx.doi.org/10.4271/2006-01-3317.